Superinsulating heat transfer surfaces for microfluidic channels

SUPERINSULATING HEAT TRANSFER SURFACES FOR MICROFLUIDIC CHANNELS

G.Rosengarten[1], C. Stanley[1]. F. Kwok[1]

[1] School of Mechanical and Manufacturing Engineering,
University of New South Wales, Sydney, Australia

ABSTRACT

In microreactors and lab-on-a-chip devices it is often important to heat a liquid above ambient temperature while it flows through thermally insulated microfluidic channels. In this paper we introduce, for the first time, the heat transfer analog of pressure drop reduction associated with patterned superhydrophobic (SH) surfaces, by showing how there is an also significant reduction in the convective heat transfer coefficient between the liquid and the SH surface. We use computational fluid dynamics to simulate a wide variety of surface patterns and wall thermal conductivities, and experiments to investigate the effect of SH surfaces on heat transfer rate. We demonstrate that without altering the bulk material properties the interfacial thermal resistance can be significantly increased. The effect is shown to be highly dependent on a variety of conditions including the Peclet number, the thermal conductivity of the wall and the shear free area. Under certain conditions we demonstrate heat transfer reductions of up to 67% using glass walls relative to a smooth surface Thus we call such surfaces superinsulating.

INTRODUCTION

Lab-on-a-chip or micro-total-analytical-systems (μTAS), and micro reactors often involve heating a liquid above ambient temperatures in order to control biological systems and chemical reactions. Examples of such devices include polymerase chain reaction (PCR) for DNA amplification, which requires rapid temperature cycling between 37 and 90^{o}C [1], micro fuel-cells that run at temperatures up 150 ^{o}C [2], and methanol reforming for hydrogen production which requires temperatures between 250-300^{o}C [3]. Obviously then some form of insulation is needed to minimize heat loss, increase temperature stability and decrease power consumption. It is paramount, to keep micro systems small and cheep to ensure they remain portable and affordable. Ideally then, the insulation material should be kept as thin as possible to reduce size, weight and material costs. Thus for a given material thickness the thermal resistance between the liquid in the channels and ambient should be as high as possible.

Two thermal resistances make up the total thermal resistance: 1) The resistance due to conduction through the wall of the channel (which is dictated by the thickness and thermal conductivity of the wall) and 2) the film resistance between the fluid and the inner wall of the channel. In the paper we look at increasing the resistance of the second by lowering the mean convective heat transfer coefficient using superhydrophobic surfaces.

Slip flow and superhydrophobic surfaces

Slip flow is the phenomena where the fluid velocity at a wall is not zero. It has been reasonably well documented that slip flow can reduce pressure drop, both though molecular slip on smooth surfaces [4-9], and, if a hydrophobic surface has the correct roughness scale, through shear free zones in air pockets [10-12]. Slip flow is an important phenomenon due to the fact that as the friction induced pressure drop reduces less pumping power is required. This allows for smaller cheaper pumps that require less energy to run.

While there has been a plethora of studies on molecular slip flow, both experimental and using molecular dynamics simulations, the phenomena is still not well understood and the agreement between studies is poor [7]. It is clear however, that slip lengths are generally small (< 1μm) which means that the associated pressure drop is not breathtaking (<10%). Similar percentage reductions have also been reported in the heat transfer rate with molecular slip in microchannels [9].

On the other hand, fewer studies have focused on pressure drop reduction of patterned superhydrophobic surfaces, where induced roughness means that water cannot penetrate into the small gaps below the top of the roughness. Studies have shown contact angles close to 180^o by tailoring the roughness [13]. Super/ultra-hydrophobic surfaces in microchannels have been shown in decrease the pressure drop by as much as 40% (with slip length in tens of micrometers) [10, 11]. Theoretical predictions have shown that as the channel height is decreased the reduction in pressure drop can exceed 60% [10].

It is clear then that drag reduction for microchannel flow is very useful and possible with superhydrophobic surfaces. The question then arises regarding the heat transfer. What happens to the heat transfer rate in superhydrophobic surfaces. In a very recent paper by Hodes *et al* [14] the effect of patterned superhydrophobic surfaces on the heat transfer rate was discussed. They calculated a Nusselt number based on an effective slip length that is obtained in superhydrophobic channels. This Nusselt number while in a different form is the same as that calculated by Rosengarten *et al* previously [9]. Hodes *et al* have no experimental or numerical results on the effect of superhydrophobicity on the heat transfer rate.

In this paper we show, using experiments and a series of numerical simulations, the effect that patterned superhydrophobic surfaces have on the heat transfer rate for a range of conditions and common wall materials.

NUMERICAL SIMULATIONS

The commercial computation fluid dynamics package Fluent version 6.2.16 was used to simulate the flow and heat transfer. Ideally a two-phase flow model including surface tension, like the volume of fluid (VOF) method [15] should be used to correctly take into account the interface shape and the circulation in the air pockets. However the VOF method in its current form could not be used due to the dominance of surface tension forces causing spurious parasitic currents to control the flow [16]. Instead we used a solid with the thermal conductivity of air in the pockets, with a shear free boundary at the liquid interface. This is a reasonable approximation as shown by [17] as the interface is almost flat and air circulation does not play a significant role in the pressure drop. A two dimensional mesh was used to simulate flow though a parallel plate configuration with one wall adiabatic and the outer temperature of the other wall at a uniform temperature (see Figure 1).

The continuity, momentum and energy equations were solved on a refined mesh with rectangular cells of 0.5μm around the solid/liquid interface and 2μm around the bottom of the solid base. There was a less than 2% change in the local heat flux using this grid and one with cells half the size. A second order upwind scheme was used in the discretisation of the equations. Slug flow at 20°C was used at the inlet and a uniform temperature of 40°C at the bottom of the wall.

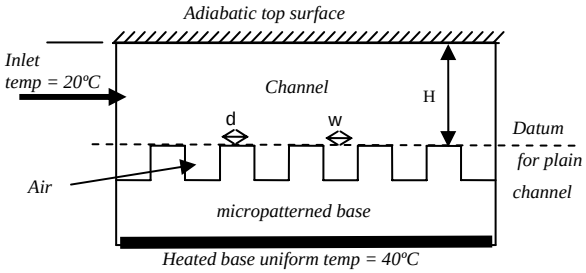

Figure 1: Schematic of 2D geometry used in numerical simulations.

EXPERIMENTS

A microchannel with a superhydrophobic heat transfer surface was fabricated in polydimethly siloxane (PDMS) using an SU8 (MicroChem) master that was fabricated on a silicon wafer using standard photolithography techniques [18]. Figure 2 shows one drop sitting on a smooth section of PDMS and the other on a patterned superhydrophobic surface. The smooth PDMS has a contact angle of deionised water of approximately 115°, while the microfabricated ridges gave a contact angle of approximately 135°.

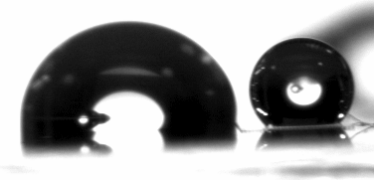

Figure 2: A droplet on a smooth PDMS surface, left and a patterned superhydrophobic surface, right.

To make the channels, a 1mm thick layer of PDMS was deposited onto the silicon substrate that had the patterned SU8 surface and the smooth surface. The 20mm long, 150μm high, 2mm wide channel was cast in 10mm thick PDMS from SU8 mold on another wafer. Holes were punched through the channel layer of the PDMS for the inlet, outlet and the pressure tapings. The channel and the bottom surface were then treated with a hand-held laboratory Corona Treater (Electro-Technic Products Model BD-20AC) to make them temporarily hydrophilic so that they could be bonded irreversibly. A 10W resistive heater was connected to a 3mm thick polished copper block. The polished copper formed a reversible bond with the PDMS. The copper block has 3 holes where 70μm thick type T thermocouples were inserted (see Figure 3). Thermocouples were also placed in the inlet and outlet of the channels. The thermocouples were calibrated against a traceable resistance thermometer. The whole arrangement was sealed in 100mm thick polystyrene insulation. A HNP Mikrosysteme mzr-2921 micropump with a bypass module was used to pump the fluid though channels and a Honeywell 26PC01Kxxa differential pressure sensor was used to measure the pressure drop. A National Instruments Ni cDAQ9172 (Ni9211 and NI 9215 modules) data acquisition system with a customized Labview program was used to collect the data.

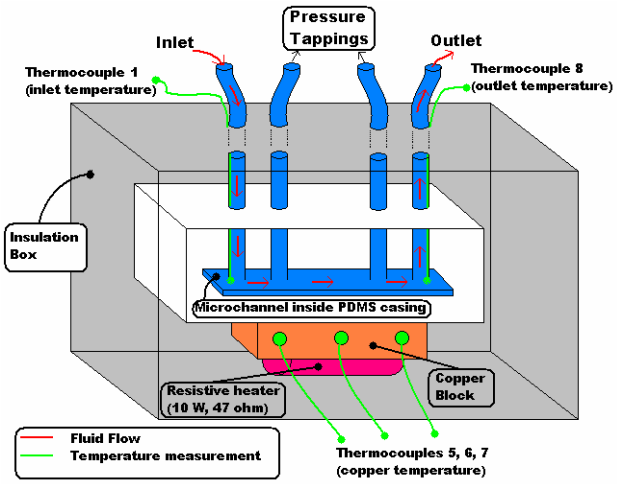

Figure 3: Schematic of test section layout.

After completion of the experiments the channel was sectioned to measure the actual dimensions. A photograph using a 20x microscope objective is shown in Figure 4. The dimensions shown in Figure 4 indicate a shear free ratio of 0.72.

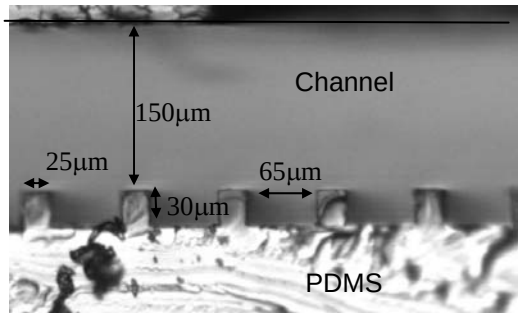

Figure 4: Cross section of superhydrophobic channel in PDMS showing the dimensions (the smooth channel was 150μm high**).**

Uncertainties

The major experimental uncertainties contributing to the over uncertainty in the experimental results are listed in Table 1.

Table 1: Uncertainties in measured quantities

Value	**Uncertainty**
Pressure	5%
Temperature	0.2°C
Flow rate	3%
Channel height, width	5μm, 10μm

RESULTS

Pressure drop

In order to validate the numerical simulations the pressure drop calculated using CFD was compared to the measured results and standard laminar flow theory (f=24/Re for parallel plates). The data is plotted in Figure 5. For the smooth channel the experiments, theory and CFD agree very well. Similarly, for the superhyrophobic surface, the pressure drop calculated with CFD agrees very well with the experimental results. The average pressure drop reduction is approximately 30% which is consistent with previous studies with a similar shear free area ratio [11].

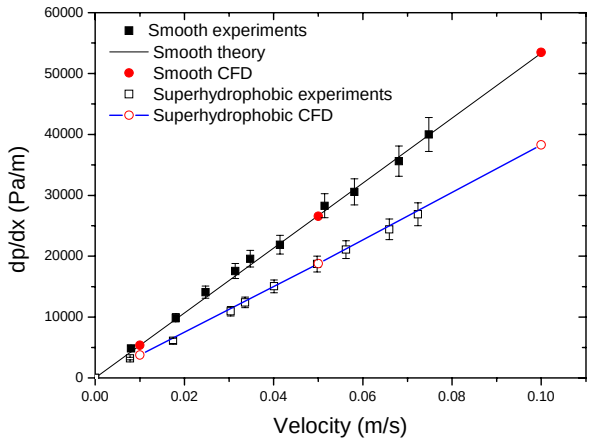

Figure 5: Pressure gradient as a function of velocity calculated from theory, experiment and CFD for smooth and superhydrophobic surfaces.

Heat transfer

Due to the low Reynolds numbers in microfluidic devices the flow may often not be fully developed. It is in the developing region that the superinsulating surfaces will have the largest effect. Additionally, especially because glasses and polymers are often used as the channel material, there may be a significant thermal resistance between the heater and the solid/fluid interface. This is indeed the case for our experimental set-up because between the heated copper block and the solid/fluid interface we had approximately 1mm thick PDMS that has a thermal conductivity of 0.18W/m.K. In order to analyze the effect of this on the heat transfer rate, we modify the one-dimensional approximation method reported by Campo and Sanchez [19] for pipe flow to be applicable to parallel plate flow.

An equivalent mean Nusselt number can be found that takes into account the wall conduction thermal resistance and the convective resistance at the wall/fluid interface. This equivalent Nusselt number, Nu_{eq}, is given by (assuming no axial conduction)

$$\frac{1}{Nu_{eq}} = \frac{1}{Nu_{Dh}} + R_w, \qquad (1)$$

where Nu_{Dh} is the standard Nusselt number based on the hydraulic diameter for flow between parallel plates with one wall isothermal and the other adiabatic. The equivalent non-dimensional wall resistance, R_w is given by

$$R_w = \frac{L/D_h}{\kappa_s/\kappa_f}. \qquad (2)$$

L is the thickness of the wall between the heat source and the fluid interface, κ_s and κ_f are the thermal conductivities of the wall and fluid respectively and D_h is the hydraulic diameter of the channel.

For the mean Nusselt number for developing flow we can use the following correlation [20]

$$Nu_{Dh} = 4.86 + \frac{0.0606 z^{*-1.2}}{1 + 0.0909 \mathrm{Pr}^{0.17} z^{*-0.7}} \qquad (3)$$

where $z^* = \frac{z/D_h}{\mathrm{Re}\,\mathrm{Pr}}$ is the non-dimensional axial distance along the channel.

It turns out [19] that the total heat transfer rate fpr developing flow can be written as

$$\frac{Q}{Q_{max}} = 1 - \exp\left(-\frac{Nu_{eq}}{\mathrm{Re}\,\mathrm{Pr}}\frac{L}{D_h}\right), \qquad (4)$$

where, given an outer wall temperature of T_{wall} and fluid inlet temperature T_{in}, Q_{max} is the maximum possible heat transfer rate given by

$$Q_{max} = \dot{m} c_p (T_{wall} - T_{in}) \qquad (5)$$

Experimental results for the smooth channel can the be compared to equation 4.

The experimental heat transfer data are plotted in Figure 6 for the smooth and superhydrophobic channels. The results for the smooth channel are in good agreement with the theoretical prediction given in equation (4) as shown by the linear least squares fit to data being close to the theoretical dotted line (based on equation (4)). The SH case shows a reduced heat transfer rate by about 18% indicated by the line of best fit. The CFD results for the same system are also plotted, but because only a 1.8mm length was modeled the Q/Q_{max} is very small. However the CFD results still show an approximately 10% difference in the heat transfer rate for this condition. For the experimental set-up, the thickness of the PDMS with a thermal conductivity of 0.18W/m.K is approximately 1mm. Therefore the thermal resistance due to conduction is about 5 times larger than the convective heat transfer due to convection. This means that for our experiments the effect of changes in the convective heat transfer coefficient is partially obscured by the larger conductive resistance. This will be addressed in further studies with thinner PDMS. In order to help elucidate the superinsulating effect we use CFD for to simulate cases with smaller wall resistances.

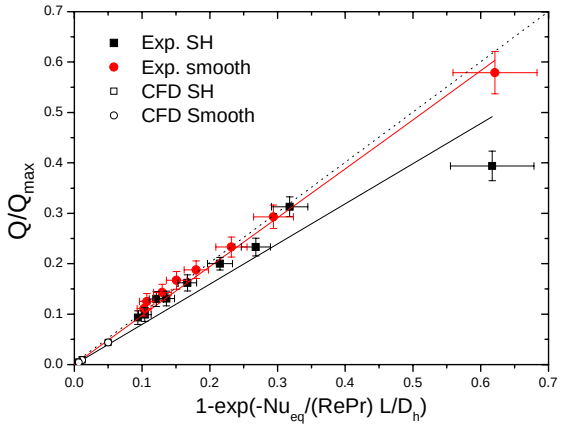

Figure 6: Experimental and CFD non-dimensional heat transfer rate plotted against theory (dotted line). The lines are linear least squares fit to the experimental data.

The CFD simulations consisted of a 90μm thick wall with a 90μm high two dimensional channel which are similar dimensions to those used by Ou *et al* [11]. A variety of configurations of two dimensional surface patterns were simulated with ridges ranging from 10 to 30μm wide (d), gaps 30 to 50μm wide (w) and ridge heights ranging from 30 to 70μm, using walls of stainless steel (κ=16W/m.K) unless otherwise mentioned. The effect of different wall thermal conductivities is discussed later.

Temperature

Out of the cases we studied the one that gave the highest reduction in heat transfer rate was the 70μm high, 10μm wide ridge with 50 μm wide air pockets. Figure 7 is a contour plot of the temperature for this superhydrophobic case and a smooth case. The temperature at the fluid/solid interface is considerably higher for the smooth case as the air gaps acts as insulators for the SH case. The ridges act as fins by creating a low resistance path through the air gap, but only their tips are exposed to the moving water minimising their effectiveness.

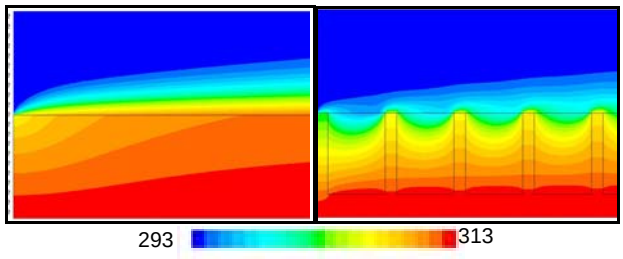

Figure 7: Temperature contours for smooth and patterned stainless steel. Vel= 0.1m/s.

This insulation effect can be seen more clearly in Figure 8 where the temperature at the solid/liquid interface is plotted as a function of distance along the channel, for both the smooth and SH cases. Clearly the mean temperature of the SH surface is less than the flat surface due to the increased thermal resistance of the SH surface. However the SH surface temperature oscillates corresponding to the regions of solid and air. This has been highlighted in the inset of Figure 8 which shows the large temperature increase corresponding to the stainless steel ridges.

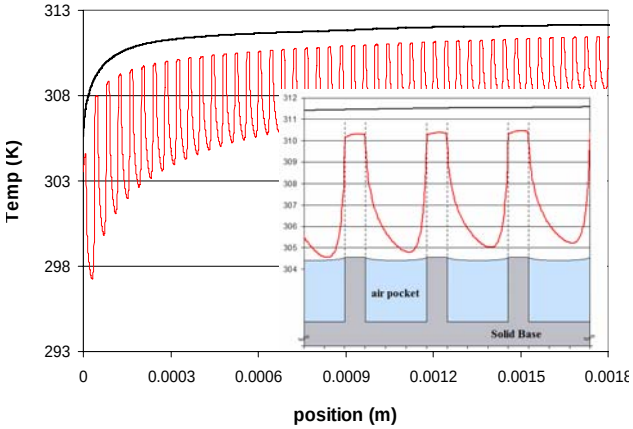

Figure 8: Temperature along surface of channel for smooth and hydrophobic surface. Vel =0.1m/s.

Local heat transfer rate

The effect of the SH surface on the local heat transfer coefficient is shown in Figure 9. An interesting phenomenon occurs that causes a decrease in the insulating properties of the SH surface. The inset graph shows this more clearly. At each ridge there is a large increase in the local heat transfer due to locally developing flow where the flow changes from essentially slip flow over the air pockets to standard no-slip conditions over the ridges. Additionally there is an increase in the heat transfer rate at the downstream end of the ridge due to acceleration of the fluid towards the next no-slip air pocket and the larger temperature gradients around the corners of the ridge. In some cases, depending on ridge size, velocity etc, the average heat transfer rate can be higher for the SH surface due to this

effect. However as can be seen, the heat transfer coefficient at the air interface is very low (almost zero) so the overall heat transfer rate depends on, amongst other things, the shear free area ratio.

.

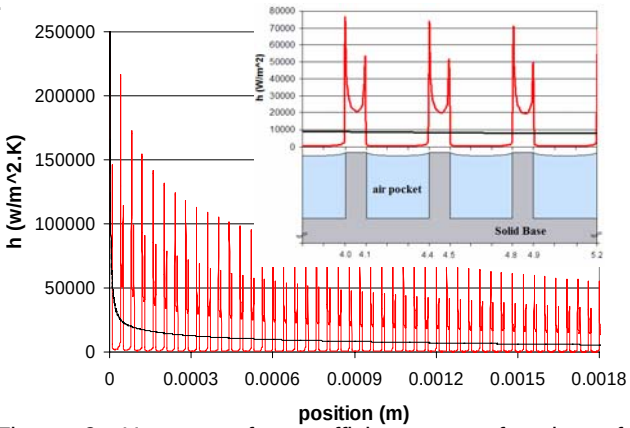

Figure 9: Heat transfer coefficient as a function of distance along channel

Shear free area

If there was no developing flow on each ridge one would expect there to be some kind of linear relationship between the heat transfer reduction and the proportion of heat transfer surface occupied by the air. The proportion is defined as the shear free area ratio, β, and is defined as

$$\beta = \frac{A_{total} - A_{no-slip}}{A_{no-slip}} = \frac{w}{d+w} \qquad (6)$$

where A is the surface area of the wall/fluid interface and w and d are defined in Figure 1. Figure 10 shows the dependence of the heat transfer rate reduction on the shear free area ratio and on the height of the ridge. There is a near linear dependence of the heat transfer reduction with the shear free area ratio with some minor undulations due to different sizes of the air gap. Similarly as would be expected higher ridges mean a thicker air gap, and thus larger reductions in the heat transfer rate. This is clearly shown in the height trend in Figure 10.

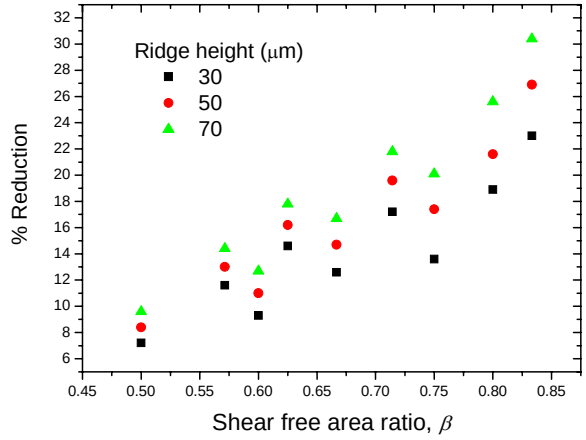

Figure 10: Heat transfer rate as a function of shear free ratio and depth of the air pocket for a stainless steel wall. Vel = 0.1m/s.

Wall thermal conductivity

To determine the effect of thermal conductivity on the heat transfer rate reduction, the case with the highest reduction in heat transfer with a stainless steel wall was modeled by replacing the thermal properties of stainless steel with those of glass (κ=1.1 W/m.K) and PDMS (κ=0.18 W/m.K) The effect of thermal conductivity on the temperature contours is shown in Figure 11. The normal to the isotherms indicates the direction of the heat transfer. Due to the relatively low thermal conductivity of PDMS there is little difference in the heat flux from the air relative to that from the ridges and the isotherms are almost parallel to the channel wall (about 50% of the heat transferred through the shear free interface). On the other hand due to the very large difference in the thermal conductivity of steel relative to air (ratio of 640) most of the heat is transferred through the ridges,only 8% is transferred through the shear-free air interface. This can be seen by the bending of the temperature contours around the ridges. Thus the higher thermal conductivity walls may be thought of as almost shorting out the effect of the SH surface.

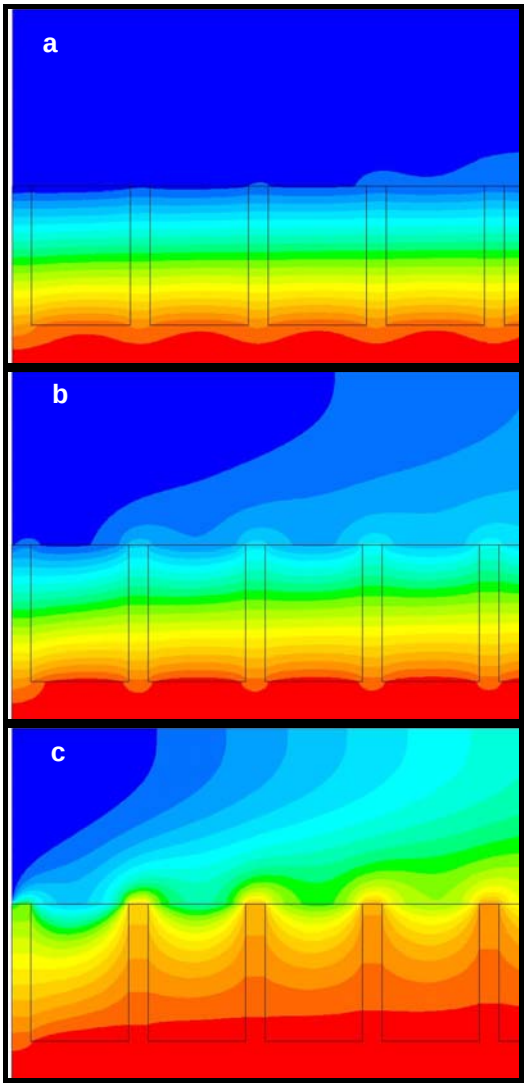

Figure 11: Temperature contours for a) PDMS, b) glass, and c) stainless steel as a function of thermal conductivity (u=0.01m/s).

A summary of the heat transfer rate results for different velocities and wall thermal conductivities is shown in Table 2 for the previously discussed case with 10μm wide 70μm deep ridges and 50 μm wide air gap.

The heat transfer rates for the stainless steel cases with the lowest velocity are very close to the maximum possible heat transfer so that the reduction with a SH surface in minimal. At higher velocities where the flow is not thermally developed there is a significant increase in the heat transfer reduction as can be seen in the 0.1m/s columb. Generally the lower thermal conductivity materials gave better reductions is the heat transfer rate, which is fortuitous as one would need insulating materials in the first place to keep the heat in (the overall heat transfer rate is lower with the glass and PDMS as can be seen by the Q/Q_{max} vaules).

Table 2: Summary of heat transfer rates for different materials and flow velocities

			Mean channel velocity (m/s)		
			0.01	0.05	0.1
Steel	Smooth	Q/	0.995	0.792	0.576
	SH	Q_{max}	0.974	0.594	0.386
	% Reduction		2	25	33
PDMS	Smooth	Q/	0.516	0.141	0.0759
	SH	Q_{max}	0.241	0.054	0.0276
	% Reduction		53	62	64
Glass	Smooth	Q/	0.966	0.516	0.319
	SH	Q_{max}	0.647	0.194	0.104
	% Reduction		33	62	67

As discussed in [10] the effect of friction drag reduction is better when the groves are parallel to the flow, due to the continuously re-developing boundary layer on the posts with transverse groves. Also in a real system there will be some air recirculation in between the ridges which will aid heat transfer. There will be a smaller effect of this recirculation on the heat transfer when there are long parallel groves. Thus we would expect a larger heat transfer reduction when the groves are parallel and thus better performance for superinsulating surfaces.

CONCLUSION

We have shown that given the right conditions patterned superhydrophobic surfaces can significantly increase the thermal resistance between a solid and liquid due to the insulating properties of the trapped air. We have shown using CFD that reductions of over 60% in the heat transfer rate relative to smooth surfaces are possible with non-metal surfaces. A stainless steel superhydrophobic surface still had reductions of around 30% but this was highly flow dependant. The heat transfer reduction is highly dependant on the shear free area ratio. We have shown that properly designed superhydrophobic surfaces have the potential to be used as superinsulators in microdevices where significant material can be saved to achieve the same thermal resistance as that for standard smooth surfaces. Further work is still required however to fully characterize and predict the effect of different surface topologies on the heat transfer rate to help design optimal systems.

ACKNOWLEDGMENTS

We thank Meng Chong for fabrication of the SU8 mold

REFERENCES

1. Lee, D., S. Park, H. Yang, K. Chung, T. Yoon, S. Kim, K. Kim, and Y. Kim, Bulk-micromachined submicroliter-colume PCR chip with very rapid thermal response and low power consumption. *Lab on a Chip*, 4. 401-409 (2004).
2. Faghri, A. and Z. Guo, Challenges and opportunities of thermal management issues related to fuel cell technology and modelling. *International Journal of Heat and Mass Transfer*, 48. 3891-3920 (2005).
3. Reuse, P., A. Renken, K. Haas-Santo, O. Gorke, and K. Schubert, Hydrogen production for fuel cell applications in an autothermal micro-channel reactor. *Chemical Engineering Journal*, 101(1-3). 133-141 (2004).
4. Barrat, J. and L. Bocquet, Large Slip effect at a Nonwetting Fluid-Solid Interface. *Physical Review Letters*, 82(3). 4671-4674 (1999).
5. Boudry, J. and E. Charlaix, Experimental Evidence for a Large Slip Effect at a Nonwetting Fluid-Solid Interface. *Langmuir 2001*, 17. 532-5236 (2001).
6. Choi, C., K. Westin, and K. Breuer. *To slip or not to slip-water flow in hydrophilic and hydrophobic microchannels*. in *International Mechanical Engineering conference and exposition*. New Oreans.(2002).
7. Lauga, E., M. Brenner, and H. Stone, *Microfluidics: The No-Sip Boundary Condition*, in *Handbook of Experimental Fluid Dynamics*, J. Foss, C. Tropea, and A. Yarin, Editors. 2005, Springer: New York.
8. Tretheway, D. and C. Meinhart, Apparent fluid slip at hydrophobic microchannel walls. *Physics of Fluids*, 14(13). 9-12 (2002).
9. Rosengarten, G., J. Cooper-White, and G. Metcalfe, Experimental and analytical study of the effect of contact angle on liquid convective heat transfer in microchannels. *International Journal of Heat and Mass Transfer*, 49(21-22). 4161-4170 (2006).
10. Chang-Hwan, C., U. Umberto, K. Joonwon, H. Chih-Ming, and K. Chang-Jin, Effective slip and friction reduction in nanograted superhydrophobic microchannels. *Physics of Fluids*, 18(8). 087105 (2006).
11. Ou, J., B. Perot, and J.P. Rothstein, Laminar drag reduction in microchannels using ultrahydrophobic surfaces. *Physics of Fluids*, 16(12). 4635-4643 (2004).
12. Watanbe, K., Yanuar, and H. Udagawa, Drag reduction of Newtonian fluid in a circular pipe with a highly water-repellent wall. *Journal of Fluid Mech.*, 381. 225-238 (1999).
13. Chen, W., A.Y. Fadeev, M.C. Hsieh, D. Oner, J. Youngblood, and T.J. McCarthy, Ultrahydrophobic and Ultralyophobic Surfaces: Some Comments and Examples. *Langmuir*, 15(10). 3395-3399 (1999).
14. Hodes, M., R. Enright, C. Eason, T. Dalton, T. Salamon, P. Koldner, and T. Krupenkin. *Friction factors and Nusselt numbers in microchannels with superhydrophobic walls*. in *Fourth International*

Conference on Nanochannels, Microchannels and MiniChannels. Limerick, Ireland.(2006).
15. Hirt, C.W. and B.D. Nichols, Volume of Fluid (VOF) Method for the Dynamics of Free Boundaries. *Journal of Computational Physics*, 39. 201-225 (1981).
16. Harvie, D., M. Davidson, and M. Rudman, An analysis or parasitic current generation in Volume of Fluid simulations. *Applied Mathematical Modelling*, 30(10). 1056-1066 (2006).
17. Ou, J. and J. Rothstein, Direct velocity measurements of the flow past drag-reducing ultrahydrophobic surfaces. *Physics of Fluids*, 17(10). 103606 (2005).
18. Nguyen, N. and S. Wereley, *Fundamentals and Applications of Microfluidics*: Artech House.(2002)
19. Campo, A. and A. Sanchez, Convective Heat Transport of High-pressure flows inside active, thick walled tubes with isothermal outer surfaces: usage of Nusselt correlation equations for an inactive, thin walled-tube. . *Applied Thermal Engineering*, 18(3-4). 257-169 (1998).
20. Mercer, W., W. Pearce, and J. Hitchcock, Laminar forced convection in the entrance region between parallel flat plates. *ASME Journal of Heat Transfer*, 89. 251-257 (1967).